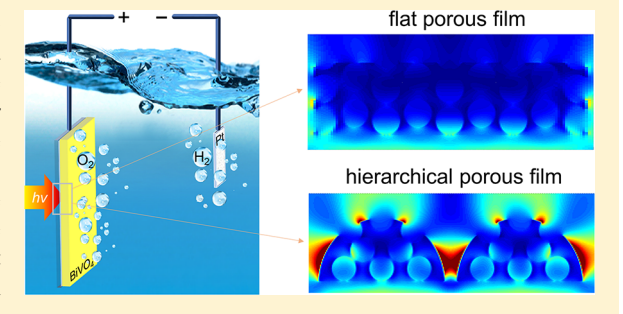
# Highly Efficient Photoelectrochemical Water Splitting from Hierarchical WO<sub>3</sub>/BiVO<sub>4</sub> Nanoporous Sphere Arrays

Yangen Zhou,<sup>†,‡</sup> Leyuan Zhang,<sup>†</sup> Linhan Lin,<sup>†</sup> Bryan R. Wygant,<sup>§</sup> Yang Liu,<sup>§</sup> Yue Zhu,<sup>†</sup> Yuebing Zheng,<sup>†</sup> C. Buddie Mullins,<sup>§</sup> Yu Zhao,<sup>\*,‡</sup> Xiaohong Zhang,<sup>\*,‡</sup> and Guihua Yu<sup>\*,†</sup>

Supporting Information

ABSTRACT: Nanoarchitecture of bismuth vanadate (BiVO<sub>4</sub>) photoanodes for effectively increasing light harvesting efficiency and simultaneously achieving high charge separation efficiency is the key to approaching their theoretic performance of solar-driven water splitting. Here, we developed hierarchical BiVO<sub>4</sub> nanoporous sphere arrays, which are composed of small nanoparticles and sufficient voids for offering high capability of charge separation. Significantly, multiple light scattering in the sphere arrays and voids along with the large effective thickness of the BiVO<sub>4</sub> photoanode induce efficient light harvesting. In addition, attributed to ultrathin two-dimensional Bi<sub>2</sub>WO<sub>6</sub> nanosheets as the precursor, the synergy of various



enhancement strategies including WO<sub>3</sub>/BiVO<sub>4</sub> nanojunction formation, W-doping, and oxygen vacancy creation can be directly incorporated into such a unique hierarchical architecture during the one-step synthesis of BiVO<sub>4</sub> without complex pre- or posttreatment. The as-obtained photoanode exhibits a water splitting photocurrent of 5.5 mA cm<sup>-2</sup> at 1.23 V versus RHE under 1sun illumination, among the best values reported up-to-date in the field.

KEYWORDS: Hierarchical structure, photoelectrochemical water splitting, bismuth vanadate, nanoporous, oxygen vacancy

B ismuth vanadate (BiVO<sub>4</sub>) has been widely studied as the top-performer among various metal oxide photoanode materials owing to its relatively narrow bandgap of 2.4 eV, excellent stability against photocorrosion, and low cost. 1-7 The theoretical maximum water oxidation photocurrent  $(J_{max})$  for BiVO<sub>4</sub> photoanodes under standard Air-Mass 1.5 Global (AM 1.5G) solar light illumination is 7.5 mA cm<sup>-2.2,4</sup> However, the experimental water oxidation photocurrents  $(J_{PEC})$  reported to date are well below the theoretical value.  $^{5,8-10}$  The  $I_{PEC}$  is determined by light harvesting efficiency  $(\phi_{abs})$ , charge separation efficiency (yield of the photogenerated holes that reach the surface,  $\varphi_{\text{sep}}$ ), and charge transfer efficiency (yield of the surface holes that are injected into solution species,  $\varphi_{\text{trans}}$ ), which can be expressed by  $J_{\text{PEC}} = J_{\text{max}} \varphi_{\text{abs}} \varphi_{\text{sep}} \varphi_{\text{trans}}$ . In recent reports, the effective strategy of coating oxygen evolution catalysts was developed to dramatically increase the charge transfer efficiency of  $BiVO_4$  up to nearly 100%.  $^{5,13,14}$  There are also various strategies proposed to increase the charge separation efficiency of BiVO<sub>4</sub>, such as introducing nanoscale porosity, 5,8–10 thickness reduction of BiVO<sub>4</sub> film, 15–17 heterojunction construction, 9,11,18,19 elemental doping, 20–22 oxygen vacancy creation, 20,23–26 and crystal facet engineering.<sup>23,27</sup> For instance, Choi et al. have developed nanoporous network structured BiVO<sub>4</sub> photoanode composed of particles smaller than its hole diffusion length (~100 nm), <sup>28</sup> which increased the charge separation efficiency up to 90% at 1.23 V versus RHE. 5,20 Subsequently, this nanoporous structured BiVO<sub>4</sub> photoanode has been further developed by many other research groups. 5,13,14,20,29 However, the light harvesting efficiency is still low (generally below 75%), 5,11,18 which thus remains as the bottleneck to approaching the theoretic maximum performance of BiVO<sub>4</sub> photoanodes.

In order to achieve high  $\varphi_{\text{sep}}$ , the thicknesses of the photoanode are required to be small so as to shorten the carrier transfer path (Figure 1a). 5,8,17 While it is conflicting that small thickness cannot guarantee sufficient light absorption, resulting in the waste of a large portion of photons. To solve such a conflict, photoanode architectures should be rationally designed to allow multiple light scattering to prolong the optical path and simultaneously to keep a short hole diffusion

Received: October 31, 2017 Revised: November 15, 2017 Published: November 29, 2017

<sup>&</sup>lt;sup>†</sup>Materials Science and Engineering Program and Department of Mechanical Engineering, The University of Texas at Austin, Austin, Texas 78712, United States

<sup>&</sup>lt;sup>‡</sup>Institute of Functional Nano & Soft Materials (FUNSOM), Jiangsu Key Laboratory for Carbon-Based Functional Materials & Devices, Soochow University, Jiangsu 215123, China

<sup>§</sup>Department of Chemical Engineering and Department of Chemistry, Center for Electrochemistry, University of Texas at Austin, Austin, Texas 78712, United States

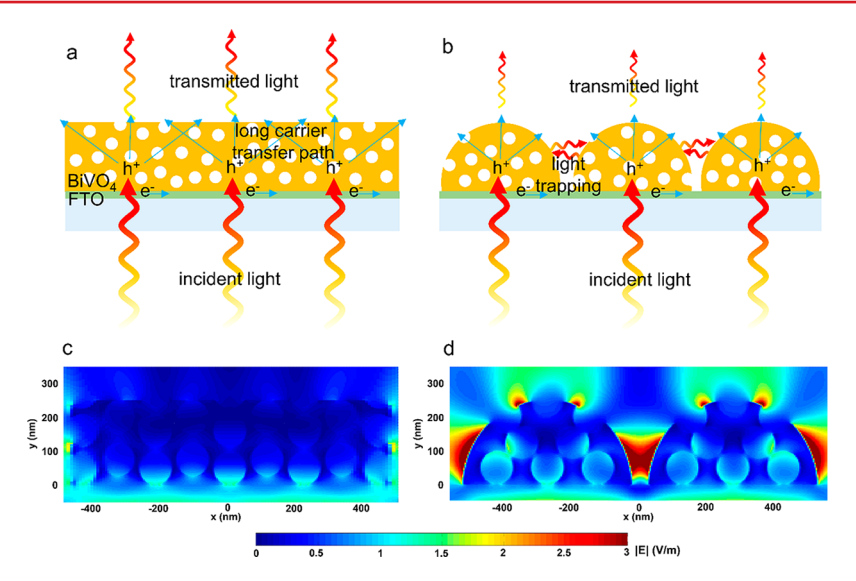


**Figure 1.** Schematic illustration of the optical absorption and charge carrier transport of thin-film-based BiVO<sub>4</sub> photoanode with porous structures: (a) flat BiVO<sub>4</sub> film and (b) hierarchical BiVO<sub>4</sub> nanostructured film composed of sphere arrays. Compared with flat BiVO<sub>4</sub> film with identical thickness, the hierarchical BiVO<sub>4</sub> film composed of sphere arrays exhibits shorter carrier transfer path. Moreover, multiple light scattering both within the voids and among the spheres can take place within the film, leading to decreased recombination rate of electron—hole pairs in the flat BiVO<sub>4</sub> film composed of sphere arrays. (c,d) Comparison of simulated cross-sectional electric field intensity, |E|, distribution of the electromagnetic wave at 420 nm in flat BiVO<sub>4</sub> film and hierarchical BiVO<sub>4</sub> film composed of sphere arrays, respectively. The thickness of BiVO<sub>4</sub> film and the void diameter are set to 250 and 100 nm, respectively, in the simulation.

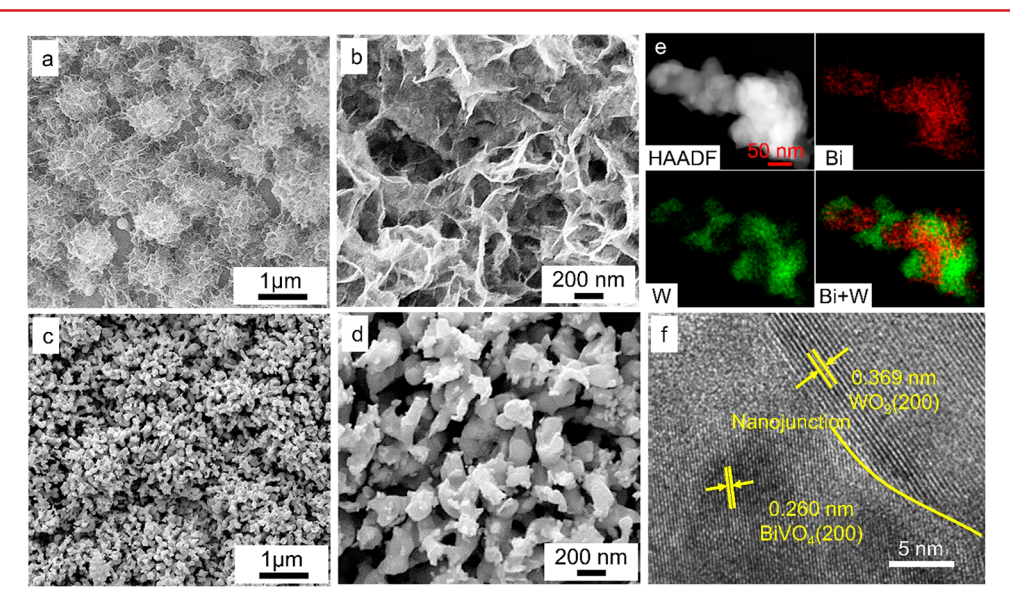


Figure 2. (a,b) SEM images of  $Bi_2WO_6$  microflower arrays assembled from ultrathin nanosheets; (c,d) SEM images of hierarchical  $WO_3/BiVO_4$  film; (e) STEM image and elemental mapping of particle from hierarchical  $WO_3/BiVO_4$  film; (f) HRTEM image of nanoparticle from hierarchical  $BiVO_4$  nanostructured film.

path. 8-10 Two types of BiVO<sub>4</sub> photoanode architectures have been reported, only which can achieve photocurrent densities much higher than 5 mA cm<sup>-2</sup> at 1.23 V vs RHE under one sun illumination so far (see Table S1 in Supporting Information). 8-10 The first type is to coat a thin BiVO<sub>4</sub> absorber layer with thickness smaller than the carrier diffusion length on nanostructured arrays to form heterojunction structure. 9,10 The thin nature of the BiVO<sub>4</sub> absorber as well as the heterojunction structure guarantees high charge separation efficiency, while the high aspect ratio of the nanostructured arrays allow multiple light scattering for high light harvesting efficiency. The second type proposed by Cui et al. is to deposit a thick nanoporous BiVO<sub>4</sub> layer onto unique nanostructured arrays. The thick

nanoporous  ${\rm BiVO_4}$  layer maintains highly efficient charge separation, while nanostructured arrays induce multiple light scattering for enhancing light trapping.

In this study, we proposed hierarchical BiVO<sub>4</sub> nanoporous sphere arrays for efficient solar water splitting, which are composed of particles smaller than its hole diffusion length and sufficient voids for guaranteeing high  $\varphi_{\rm sep}$ . The multiple light scattering in the microsphere arrays and voids along with a large thickness of BiVO<sub>4</sub> photoanode ( $\sim$ 1.3  $\mu$ m) results in high  $\varphi_{\rm abs}$  (Figure 1b). To easily prepare the hierarchical BiVO<sub>4</sub> nanoporous sphere arrays composed of small nanoparticles and sufficient voids, ultrathin Bi<sub>2</sub>WO<sub>6</sub> nanosheets-assembled microflower arrays were developed as the precursor. It is worth

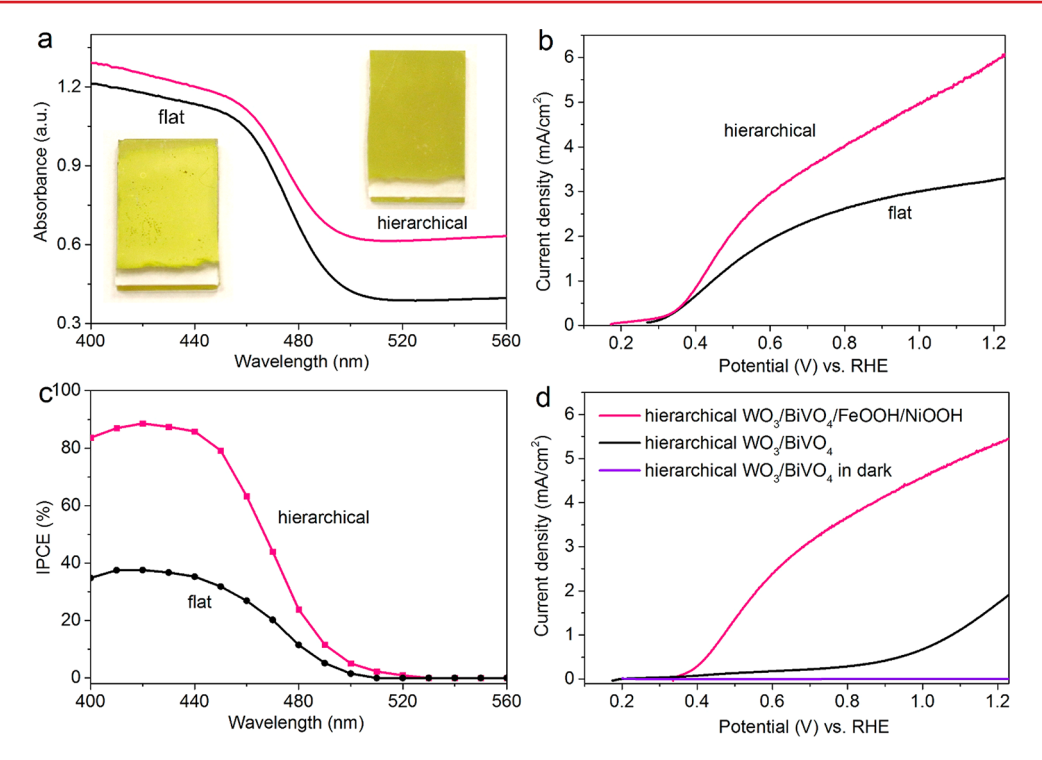


Figure 3. (a) UV–vis DRS (inset: photographs of samples) and (b) photoelectrochemical activities for sulfite oxidation of nanoporous WO<sub>3</sub>/BiVO<sub>4</sub> electrodes with hierarchical structure and flat structure, measured in a 0.5 M phosphate buffer (pH 7) containing 0.5 M Na<sub>2</sub>SO<sub>3</sub> under AM 1.5 G, 100 mW cm<sup>-2</sup> illumination with a scan rate of 20 mV s<sup>-1</sup>. (c) IPCE of hierarchical WO<sub>3</sub>/BiVO<sub>4</sub> photoanode measured in the same solution at 1.23 V vs RHE. (d) Effect of oxygen evolution catalyst on photocatalytic water oxidation performance of hierarchical WO<sub>3</sub>/BiVO<sub>4</sub> electrode, measured in a 0.5 M phosphate buffer (pH 7) under AM 1.5 G.

noting that in addition to the architecture designed for increasing  $\varphi_{abs}$ , multiple strategies are indispensable for guaranteeing high  $\varphi_{sep}$  and  $\varphi_{trans}$  of BiVO<sub>4</sub> photoanodes (see Table S1). Importantly, several enhancement strategies including formation of WO<sub>3</sub>/BiVO<sub>4</sub> nanojunction, creation of oxygen vacancies, and W-doping can be simultaneously and readily incorporated in the hierarchical architecture during the one-step preparation of BiVO<sub>4</sub> from the two-dimensional (2D) material Bi<sub>2</sub>WO<sub>6</sub>, without complex pre- or post-treatment. As 2D materials possess attractive structure-derived properties and offer opportunities to tackle challenges in many energy-related technologies, <sup>30,31</sup> this work presents unique advantages of 2D materials as precursor for preparation of new functional materials.

To shed light on the light trapping mechanism of hierarchical BiVO<sub>4</sub> nanoporous sphere arrays, optical absorption simulations on both flat and hierarchical BiVO<sub>4</sub> nanoporous films were performed. The cross-sectional electric field intensity distributions of the electromagnetic wave at 420 nm over the two samples are plotted in Figure 1c,d. For the flat nanofilm, the electric field intensity was evenly distributed in the bulk. However, for the hierarchical BiVO<sub>4</sub> nanoporous film, as the distance between nanosphere arrays approaches the wavelength of incident light, the incident light is scattered and trapped in the nanosphere arrays. The areas between adjacent nanosphere arrays exhibit an intensified electric field, corresponding to light trapping in these areas. The simulation results support that the nanoporous sphere arrays are able to contribute to light trapping for increasing light harvesting efficiency.

In terms of synthesis,  ${\rm Bi_2WO_6}$  nanosheets as precursors for the preparation of nanoporous  ${\rm BiVO_4}$  were grown on F-doped  ${\rm SnO_2}$  (FTO)-coated glass substrates by a modified self-

assembly approach (see Experimental Section in the Supporting Information).<sup>32</sup> The as-prepared Bi<sub>2</sub>WO<sub>6</sub> (Figure 2a,b and Figure S1) is shown to be microflower arrays assembled by ultrathin nanosheets. The microflowers are  $1-2 \mu m$  in diameter and are closely packed. X-ray diffraction (XRD) patterns (Figure S2) confirm that the as-obtained microflower arrays were pure-phase Bi<sub>2</sub>WO<sub>6</sub>. <sup>32</sup> As a reference, a flat film composed of Bi<sub>2</sub>WO<sub>6</sub> nanosheets on FTO were also prepared (Figure S3). Conversion from the Bi<sub>2</sub>WO<sub>6</sub> nanosheets into WO<sub>3</sub>/BiVO<sub>4</sub> heterojunction was carried out by annealing the precursor under an atmosphere of vaporized vanadium acetylacetonate (V(acac)<sub>3</sub>) in a chemical vapor deposition process (Figure S4). This is different from the commonly used method to prepare a WO<sub>3</sub>/BiVO<sub>4</sub> heterojunction in which a BiVO<sub>4</sub> thin film is coated on a WO<sub>3</sub> substrate. 9-11,19,33 As evidenced by the XRD pattern in Figure S5, pure-phase WO<sub>3</sub> and BiVO<sub>4</sub> are formed after calcination in air. Figure 2c,d and Figure S6 suggest that the Bi<sub>2</sub>WO<sub>6</sub> microflower arrays converted into nanoporous sphere arrays after calcination. This hierarchical nanostructured film on FTO has a thickness of  $\sim 1.3 \mu m$  (Figure S7). The ultrathin Bi<sub>2</sub>WO<sub>6</sub> nanosheets as precursors can result in small size of the BiVO<sub>4</sub> nanoparticles and the WO<sub>3</sub> nanoparticles. Therefore, the hierarchical structured film with abundant exposed active sites on the surface would have efficient mass transfer and thus high photocatalytic activity. A flat WO<sub>3</sub>/ BiVO<sub>4</sub> nanoporous film with a thickness of  $\sim$ 1.3  $\mu$ m was also prepared from the flat Bi<sub>2</sub>WO<sub>6</sub> film (Figure S2).

We further carried out element mapping analysis to characterize the WO<sub>3</sub>/BiVO<sub>4</sub> heterojunction in the nanoporous film. Figure 2e and Figure S8 indicate that the small nanoparticles in the hierarchical structure are the assembly of many smaller nanoparticles with irregular shape. Moreover, the

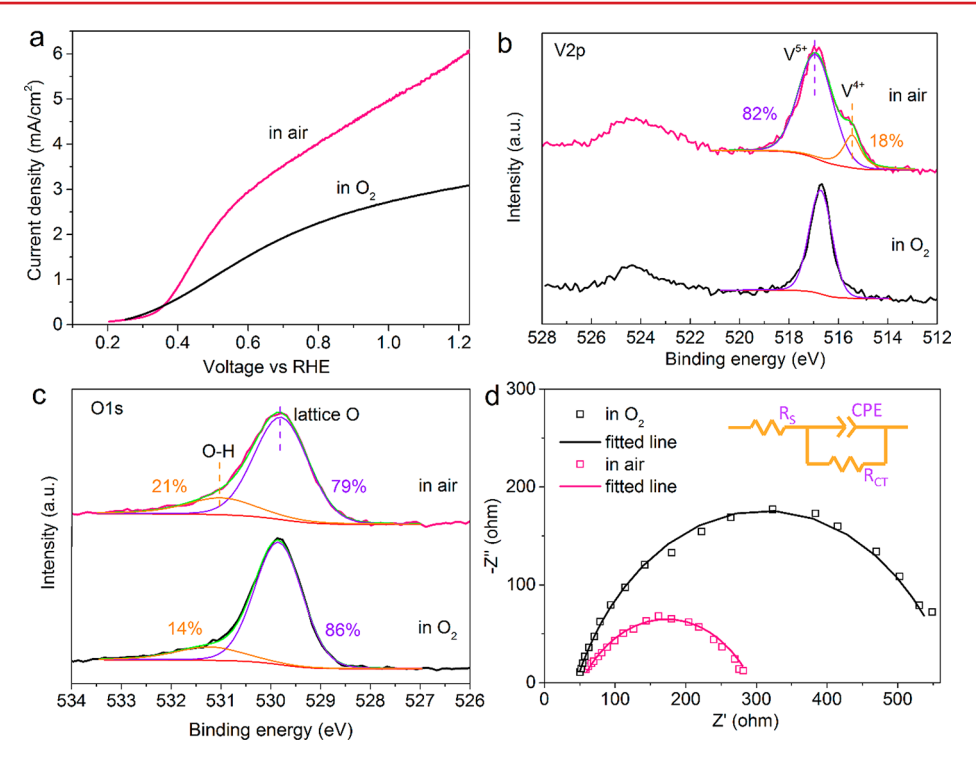


Figure 4. (a) Photoelectrochemical activities, (b,c) XPS spectra, and (d) EIS curves (inset: equivalent circuit) of hierarchical WO<sub>3</sub>/BiVO<sub>4</sub> films prepared by calcination in air and in O<sub>2</sub>. The photoelectrochemical activities were measured in a 0.5 M phosphate buffer (pH 7) containing 0.5 M Na<sub>2</sub>SO<sub>3</sub> under AM 1.5 G illumination.

sizes of the small nanoparticles are much smaller than the hole diffusion length. The WO<sub>3</sub> nanoparticles are tightly intertwined with the BiVO<sub>4</sub> nanoparticles, indicating the formation of nanojunction between them. HRTEM image further confirms the nanojunction structure (Figure 2f). The nanoscale heterojunction between nanoparticles may separate charges more effectively than the commonly reported planar-like heterojunctions. 9-11 In addition, since W-doping is a widely used and effective strategy to enhance the performance of BiVO<sub>4</sub> through increasing the conductivity of charges in 18,22,34 it is interesting to find that a small amount of W atoms have been doped and distributed in the region of the BiVO<sub>4</sub> phase. During the formation of the WO<sub>3</sub>/BiVO<sub>4</sub> heterojunction, the ultrathin Bi<sub>2</sub>WO<sub>6</sub> nanosheets decomposed in situ into BiVO<sub>4</sub> and WO<sub>3</sub>. As a result, WO<sub>3</sub>/BiVO<sub>4</sub> nanojunctions and W-doping, both of which could enhance charge separation (Figure S9), can simply be achieved by the one-step calcination process.

Optical properties of the flat and hierarchical WO<sub>3</sub>/BiVO<sub>4</sub> films on FTO were measured by UV—vis diffuse reflectance spectroscopy (DRS, Figure 3a). Owing to the array structure induced multiple light scattering, the hierarchical film can adsorb more photons than the flat film. This was further indicated by the photographs of the two samples. It should be noted that the hierarchical structure caused a redshift of the absorbance edge, indicating that the photons with larger wavelength can be exploited by the hierarchical nanostructured film for photocatalytic reactions.

The photoelectrochemical properties of the flat and hierarchical WO<sub>3</sub>/BiVO<sub>4</sub> photoanodes were investigated via the photoelectrochemical oxidation reaction of sulfite, due to the significantly faster kinetics of sulfite oxidation relative to water oxidation. <sup>5,8,20</sup> As presented in Figure 3b, the hierarchical film exhibits a better photocatalytic activity than the flat film.

The onset potentials of photocurrent for the two photoanodes are almost the same. Both samples have a rapid increase in photocurrent in the range of 0.3-0.6 V vs RHE and then a slow increase in photocurrent when the potential exceeds 0.6 V vs RHE. The hierarchical sample generates a photocurrent density of 6 mA cm<sup>-2</sup> at 1.23 V vs RHE, while the flat sample generates only 3.4 mA cm<sup>-2</sup> at the same potential. The hierarchical photoanode at such a large thickness ( $\sim$ 1.3  $\mu$ m) can have a high solar water splitting performance, indicating the effective thickness of BiVO<sub>4</sub> photoanode is much higher than previously reported.<sup>8,17,29</sup> The incident photon-to-electron conversion efficiency (IPCE) was measured to determine the onset of photoabsorption for photocurrent generation and the efficiency of charge separation. <sup>20</sup> Since the kinetics of sulfite oxidation are fast, surface electron—hole recombination is negligible during photooxidation of sulfite. <sup>5,20</sup> As a result, the IPCE calculated based on the photooxidation of sulfite can provide a more accurate estimation of photocurrent onset than that based on photooxidation of water. As shown in Figure 3c, the IPCE is between 80 and 90% with wavelengths between 400 and 450 nm for the hierarchical film, compared with less than 40% for the flat film. The onset of photocurrent of the hierarchical film is located at 520 nm, 10 nm higher than that of the flat film, consistent with the DRS results.

The abilities of hierarchical BiVO<sub>4</sub> nanoporous films for photoelectrochemical water splitting were tested in a 0.5 M phosphate buffer (pH 7). It is clear in Figure 3d that the oxygen evolution catalyst FeOOH/NiOOH dramatically increases the photoelectrochemical water splitting performance of the hierarchical BiVO<sub>4</sub> anode. This is because the BiVO<sub>4</sub>/FeOOH interface can minimize electron—hole recombination, and the NiOOH/electrolyte interface makes surface charge separation more favorable while concurrently improving the water oxidation kinetics.  $^{5,10,20}$  Therefore, the dual catalyst layer

is indispensable for the significant photocurrent of solar water splitting up to 5.5 mA cm $^{-2}$  at 1.23 V vs RHE under 1-sun illlumination. The maximum applied bias photon-to-current efficiency (ABPE, Figure S10) of the hierarchical photoanode calculated from its J-V curve, assuming 100% Faradaic efficiency, is about 1.65%. In addition, the hierarchical photoanode shows good stability (Figure S11).

It should be noted that during the preparation of  $WO_3/BiVO_4$  nanoporous samples,  $O_2$  gas was consumed to convert  $V^{3+}$  of  $V(acac)_3$  into  $V^{5+}$  in  $BiVO_4$ . That means if the  $V^{3+}$  species were not completely oxidized, some V atoms would be in a low valence state in the prepared  $BiVO_4$  photoanodes. In this case, oxygen vacancies would be formed for the charge balance. Oxygen vacancies are believed to be effective for improving the bulk and surface charge separation efficiency of  $BiVO_4$ . As shown in Figure 4a, the hierarchical  $BiVO_4$  anode calcinated in  $O_2$  exhibits much lower photoelectrochemical performance than the sample calcinated in air, indicating the photocatalytic activity might be sensitive to the amount of oxygen vacancies induced by calcination with different  $O_2$  concentration.

To confirm this, X-ray photoelectron spectroscopy (XPS) spectra of the hierarchical BiVO<sub>4</sub> samples prepared in air and in O2 were acquired. As shown in Figure 4b, the XPS signal at 515.7 eV of the hierarchical WO<sub>3</sub>/BiVO<sub>4</sub> sample prepared in air reveals the existence of V<sup>4+</sup> species. 35,36 Quantitative analysis of XPS intensities indicates that ~18% of V atoms in the sample prepared in air are V4+ species. The V atoms in low valence state induce excess electrons in the BiVO<sub>4</sub> crystal, resulting in a larger number of oxygen vacancies on the surface of the sample prepared in air. 35,36 In contrast, no V4+ species could be found on the sample calcinated in O2. It should be noted that the abundant oxygen vacancies on surface could adsorb water to form a large amount of surface hydroxyl groups via dissociation of water molecules. <sup>35–37</sup> Indeed, as presented in Figure 4c, the sample prepared in air shows more surface hydroxyl groups than the sample prepared in O2. The oxygen vacancy induced surface hydroxyl groups could enhance the surface charge transfer and separation during photocatalytic reactions.<sup>38,39</sup> Up to now, many post-treatment methods have been developed to create oxygen vacancies on BiVO<sub>4</sub> samples to enhance charge transport and separation. 20,23,24,26 In contrast, here the oxygen vacancies were created directly during the preparation of the WO<sub>3</sub>/BiVO<sub>4</sub> samples.

To further understand the role of oxygen vacancies on the performance of BiVO<sub>4</sub>, electrochemical impedance spectroscopy (EIS) curves of the two hierarchical WO<sub>3</sub>/BiVO<sub>4</sub> samples that were prepared in air and in O<sub>2</sub> were measured (Figure 4d). The solid lines show fitted results according to the equivalent circuit model (inset in Figure 4d), where  $R_{\rm s}$  and  $R_{\rm ct}$  represent the series resistance and interfacial charge transfer resistance, respectively. The fitted values of each component are listed in Table S2. The  $R_{\rm s}$  for both samples are similar, indicating that the effect of series resistance is negligible. Comparing with the hierarchical WO<sub>3</sub>/BiVO<sub>4</sub> film prepared in O<sub>2</sub>, the  $R_{\rm ct}$  of the film prepared in air is much smaller, suggesting the enhancement in charge transport across the electrolyte/anode interface. This confirms again the critical role of oxygen vacancies to increase the charge transport efficiency of BiVO<sub>4</sub>.

In conclusion, we report here a rationally designed hierarchical BiVO<sub>4</sub> nanoporous sphere array as a photoanode for efficient solar-driven water splitting. The photoanode is composed of self-assembled small nanoparticles and sufficient

voids, which are beneficial to enhance the charge separation and transfer efficiencies. The hierarchical sphere array structure and the sufficient voids contribute to enhanced light harvesting efficiency by means of multiple light scattering in the photoanode and increasing effective thickness of the BiVO<sub>4</sub> photoanode. Moreover, nanojunction formation, W-doping, and oxygen vacancy creation were directly synergized in the unique architecture via a facile one-step synthetic process, which can further increase charge separation and transfer efficiencies. This material and structural design using ultrathin two-dimensional materials as the precursor present a useful strategy for fabricating hierarchically structured functional materials with excellent light-trapping and charge transfer properties.

## ASSOCIATED CONTENT

## S Supporting Information

The Supporting Information is available free of charge on the ACS Publications website at DOI: 10.1021/acs.nanolett.7b04626.

Material synthesis and characterizations, such as additional SEM images, XRD patterns and photoelectrochemical properties of the as-prepared hierarchical and flat samples, and list of performances of BiVO<sub>4</sub> photoanodes reported in literatures (PDF)

## AUTHOR INFORMATION

#### **Corresponding Authors**

\*E-mail: ghyu@austin.utexas.edu. \*E-mail: yuzhao@suda.edu.cn.

\*E-mail: xiaohong zhang@suda.edu.cn.

## ORCID ®

Yang Liu: 0000-0002-7240-1546 Yuebing Zheng: 0000-0002-9168-9477 C. Buddie Mullins: 0000-0003-1030-4801

Yu Zhao: 0000-0002-6184-2530 Xiaohong Zhang: 0000-0002-6732-2499 Guihua Yu: 0000-0002-3253-0749

#### Notes

The authors declare no competing financial interest.

# ACKNOWLEDGMENTS

G.Y. acknowledges the financial support from Welch Foundation Grant F-1861, Sloan Research Fellowship, and Camille Dreyfus Teacher-Scholar Award. C.B.M. acknowledges the financial support from Welch Foundation Grant F-1436. Y.Z. acknowledges the financial support of the National Science Foundation (1704634). Y.Z. and X.Z. acknowledge the financial support of the Six Talent Peaks Project of Jiangsu Province (BU21400316), the National Natural Science Foundation of China (51772199), the Major Research Plan of the National Natural Science Foundation of China (91333208), the National Basic Research Program of China (2012CB932400), the Collaborative Innovation Centre of Suzhou Nano Science & Technology (NANO-CIC), and the Base for Introducing Talents of Discipline to Universities (National 111 Project). Y.G.Z. acknowledges the financial support from Jiangsu Planned Projects for Postdoctoral Research Funds (1701175B).

### REFERENCES

- (1) Park, Y.; McDonald, K. J.; Choi, K.-S. Chem. Soc. Rev. 2013, 42 (6), 2321-2337.
- (2) Tolod, K.; Hernández, S.; Russo, N. Catalysts 2017, 7 (1), 13.
- (3) Sivula, K.; van de Krol, R. Nat. Rev. Mater. 2016, 1, 15010.
- (4) Kim, J. H.; Lee, J. S. Energy Environ. focus 2014, 3 (4), 339–353.
- (5) Kim, T. W.; Choi, K.-S. Science 2014, 343 (6174), 990-994.
- (6) Yang, Y.; Niu, S.; Han, D.; Liu, T.; Wang, G.; Li, Y. Adv. Energy Mater. 2017, 7 (19), 1700555.
- (7) Kuang, Y.; Jia, Q.; Ma, G.; Hisatomi, T.; Minegishi, T.; Nishiyama, H.; Nakabayashi, M.; Shibata, N.; Yamada, T.; Kudo, A.; Domen, K. *Nature Energy* **2016**, 2, 16191.
- (8) Qiu, Y.; Liu, W.; Chen, W.; Chen, W.; Zhou, G.; Hsu, P.-C.; Zhang, R.; Liang, Z.; Fan, S.; Zhang, Y.; Cui, Y. Sci. Adv. 2016, 2 (6), e1501764.
- (9) Pihosh, Y.; Turkevych, I.; Mawatari, K.; Uemura, J.; Kazoe, Y.; Kosar, S.; Makita, K.; Sugaya, T.; Matsui, T.; Fujita, D.; Tosa, M.; Kondo, M.; Kitamori, T. Sci. Rep. 2015, 5, 11141.
- (10) Shi, X.; Choi, I. Y.; Zhang, K.; Kwon, J.; Kim, D. Y.; Lee, J. K.; Oh, S. H.; Kim, J. K.; Park, J. H. Nat. Commun. **2014**, *5*, 4775.
- (11) Rao, P. M.; Cai, L.; Liu, C.; Cho, I. S.; Lee, C. H.; Weisse, J. M.; Yang, P.; Zheng, X. *Nano Lett.* **2014**, *14* (2), 1099–1105.
- (12) Zhong, D. K.; Choi, S.; Gamelin, D. R. J. Am. Chem. Soc. 2011, 133 (45), 18370–18377.
- (13) Yu, F.; Li, F.; Yao, T.; Du, J.; Liang, Y.; Wang, Y.; Han, H.; Sun, L. ACS Catal. 2017, 7 (3), 1868–1874.
- (14) Wang, Y.; Li, F.; Zhou, X.; Yu, F.; Du, J.; Bai, L.; Sun, L. Angew. Chem., Int. Ed. 2017, 56 (24), 6911–6915.
- (15) Abdi, F. F.; van de Krol, R. J. Phys. Chem. C 2012, 116 (17), 9398-9404.
- (16) Seabold, J. A.; Zhu, K.; Neale, N. R. Phys. Chem. Chem. Phys. **2014**, 16 (3), 1121–1131.
- (17) Saito, R.; Miseki, Y.; Sayama, K. J. Photochem. Photobiol., A 2013, 258, 51–60.
- (18) Abdi, F. F.; Han, L.; Smets, A. H. M.; Zeman, M.; Dam, B.; van de Krol, R. *Nat. Commun.* **2013**, *4*, 2195.
- (19) Hong, S. J.; Lee, S.; Jang, J. S.; Lee, J. S. Energy Environ. Sci. **2011**, 4 (5), 1781–1787.
- (20) Kim, T. W.; Ping, Y.; Galli, G. A.; Choi, K.-S. Nat. Commun. 2015, 6, 8769.
- (21) Luo, W.; Yang, Z.; Li, Z.; Zhang, J.; Liu, J.; Zhao, Z.; Wang, Z.; Yan, S.; Yu, T.; Zou, Z. Energy Environ. Sci. **2011**, 4 (10), 4046–4051.
- (22) He, H.; Berglund, S. P.; Rettie, A. J. E.; Chemelewski, W. D.; Xiao, P.; Zhang, Y.; Mullins, C. B. *J. Mater. Chem. A* **2014**, 2 (24), 9371–9379.
- (23) Wang, S.; Chen, P.; Yun, J. H.; Hu, Y.; Wang, L. Angew. Chem., Int. Ed. 2017, 56 (29), 8500–8504.
- (24) Trzesniewski, B. J.; Digdaya, I. A.; Nagaki, T.; Ravishankar, S.; Herraiz-Cardona, I.; Vermaas, D. A.; Longo, A.; Gimenez, S.; Smith, W. A. Energy Environ. Sci. 2017, 10 (6), 1517–1529.
- (25) Trzesniewski, B. J.; Smith, W. A. J. Mater. Chem. A 2016, 4 (8), 2919–2926.
- (26) Liu, E. Y.; Thorne, J. E.; He, Y.; Wang, D. ACS Appl. Mater. Interfaces 2017, 9 (27), 22083–22087.
- (27) Li, R.; Zhang, F.; Wang, D.; Yang, J.; Li, M.; Zhu, J.; Zhou, X.; Han, H.; Li, C. Nat. Commun. 2013, 4, 1432.
- (28) Rettie, A. J. E.; Lee, H. C.; Marshall, L. G.; Lin, J.-F.; Capan, C.; Lindemuth, J.; McCloy, J. S.; Zhou, J.; Bard, A. J.; Mullins, C. B. *J. Am. Chem. Soc.* **2013**, *135* (30), 11389–11396.
- (29) Kuang, Y.; Jia, Q.; Nishiyama, H.; Yamada, T.; Kudo, A.; Domen, K. Adv. Energy Mater. 2016, 6 (2), 1501645.
- (30) Bonaccorso, F.; Colombo, L.; Yu, G.; Stoller, M.; Tozzini, V.; Ferrari, A. C.; Ruoff, R. S.; Pellegrini, V. Science 2015, 347 (6217), 1246501.
- (31) Fang, Z.; Peng, L.; Lv, H.; Zhu, Y.; Yan, C.; Wang, S.; Kalyani, P.; Wu, X.; Yu, G. ACS Nano **2017**, 11 (9), 9550–9557.
- (32) Zhou, Y.; Zhang, Y.; Lin, M.; Long, J.; Zhang, Z.; Lin, H.; Wu, J. C. S.; Wang, X. Nat. Commun. 2015, 6, 8340.

(33) Pihosh, Y.; Turkevych, I.; Mawatari, K.; Asai, T.; Hisatomi, T.; Uemura, J.; Tosa, M.; Shimamura, K.; Kubota, J.; Domen, K.; Kitamori, T. *Small* **2014**, *10* (18), 3692–3699.

- (34) Berglund, S. P.; Rettie, A. J. E.; Hoang, S.; Mullins, C. B. *Phys. Chem. Chem. Phys.* **2012**, *14* (19), 7065–7075.
- (35) An, X.; Li, T.; Wen, B.; Tang, J.; Hu, Z.; Liu, L.-M.; Qu, J.; Huang, C. P.; Liu, H. Adv. Energy Mater. 2016, 6 (8), 1502268.
- (36) Zhang, Y.; Guo, Y.; Duan, H.; Li, H.; Sun, C.; Liu, H. Phys. Chem. Chem. Phys. 2014, 16 (44), 24519-24526.
- (37) Schaub, R.; Thostrup, P.; Lopez, N.; Lægsgaard, E.; Stensgaard, I.; Nørskov, J. K.; Besenbacher, F. *Phys. Rev. Lett.* **2001**, 87 (26), 266104.
- (38) Turchi, C. S.; Ollis, D. F. J. Catal. 1990, 122 (1), 178-192.
- (39) Kim, J.; Hwang, D. W.; Kim, H. G.; Bae, S. W.; Lee, J. S.; Li, W.; Oh, S. H. *Top. Catal.* **2005**, 35 (3), 295–303.
- (40) Lv, X.; Nie, K.; Lan, H.; Li, X.; Li, Y.; Sun, X.; Zhong, J.; Lee, S.-T. *Nano Energy* **2017**, 32, 526–532.